Monitoring the seasonal changes of an englacial conduit network using repeated ground penetrating radar measurements

Gregory Church[1,2], Melchior Grab[1,2], Cédric Schmelzbach[2], Andreas Bauder[1], and Hansruedi Maurer[2]

[1]Laboratory of Hydraulics, Hydrology and Glaciology (VAW), ETH Zurich, Zurich, Switzerland
[2]Institute of Geophysics, ETH Zurich, Zurich, Switzerland

Correspondence: Gregory Church (church@vaw.baug.ethz.ch)

Abstract. Between 2012 and 2019, repeated 25 MHz ground penetrating radar (GPR) surveys were carried out over an active englacial conduit network within the ablation area of the temperate Rhonegletscher, Switzerland. In 2018 and 2019 the repetition survey rate was increased to monitor seasonal variations. The resulting GPR data were processed using an impedance inversion workflow to compute GPR reflection coefficients and layer impedances, which are indicative of the conduit's infill material. The spatial and temporal evolution of the reflection coefficients also provided insights into the morphology of the Rhonegletscher's englacial conduit network. During the summer melt seasons, we observed an active, water-filled, sediment-transporting englacial conduit network that yielded large negative GPR reflection coefficients (<-0.2). For all the GPR surveys conducted during the summer, the englacial conduit was 15-20 m wide, ~0.4 m thick, ~250 m long with a shallow inclination (2°) and having a sinusoidal shape. We speculate that such a geometry is likely the result of extensional hydraulic fracturing. Synthetic GPR waveform modelling using a thin water-filled conduit showed that a conduit thickness larger than 0.4 m (0.3 × minimum wavelength) thick can be correctly identified using 25 MHz GPR data. During the winter periods, the englacial conduit shuts down and either physically closed or becomes very thin (<0.1 m), thereby producing small negative reflection coefficients that are caused by either sediments lying within the closed conduit or water within the very thin conduit. Furthermore, the englacial conduit reactivated during the following melt season at an identical position as in the previous year.

1   Introduction

Surface meltwater is routed through the glacier's interior by englacial drainage systems, before it reaches subglacial drainage systems (Fountain and Walder, 1998; Cuffey and Paterson, 2010). Subglacial drainage systems play an important role on the dynamics of glaciers (Iken et al., 1996; Bingham et al., 2008). For example, high subglacial water pressure can lubricate the ice-bed interface, which may result in a faster sliding velocity (Iken and Bindschadler, 1986; Zwally et al., 2002). The subglacial water pressure can dramatically increase, when the drainage system does not adapt quickly enough, while surface meltwater is routed rapidly through the englacial drainage system. There is often a short time lag between the surface meltwater being present and the increase in glacier velocity (Bingham et al., 2005). Therefore, studying the seasonal evolution of an englacial drainage system throughout the melt season is key to understanding how and when they transport water to the subglacial drainage systems.

25   Depending on the temperature of the ice, there exist different mechanisms for developing englacial drainage networks. Ice below the pressure melting point (cold ice) is impermeable and until recently it was assumed that surface melt water has limited penetration within cold-ice glaciers. However, recent research has provided evidence that surface-to-bed drainage networks are present in cold ice glaciers and they are formed by three distinct mechanisms (Benn et al., 2009; Gulley, 2009). The first mechanism includes surface melt water that creates incisions on the glacier's surface, and these surface streams can become

30   englacial, if their upper levels becomes blocked or closes due to ice creep. Such englacial streams are known as 'cut-and-closure' conduits (Gulley et al., 2009a). The second mechanism for the formation of englacial conduits within cold ice, is hydraulically assisted fracture propagation (Boon and Sharp, 2003; van der Veen, 2007). Englacial conduits can develop from water filled crevasses where stressed ice and the water pressure within the fracture is large enough to overcome the fracture toughness of the surrounding ice. The third mechanism is related to the exploitation of permeable structures within the body

35   of the glacier (Gulley et al., 2009a).

    The englacial drainage network theory was originally developed for ice at the pressure melting point (temperate ice) (Shreve, 1972; Röthlisberger, 1972). Temperate ice was assumed to be permeable and this led to the theoretical model that englacial conduits form from water flowing between ice crystal boundaries within connected veins. As a result of theoretical challenges by Lliboutry (1971) and field observations by Gulley et al. (2009b) the formation mechanisms of englacial conduits within

40   temperate ice has been questioned. As within cold ice, englacial conduits seem to form as a result of hydraulically assisted fracture propagation in temperate ice (Gulley, 2009). Additionally, englacial conduits can form from the exploitation of pre-existing fractures (Fountain et al., 2005; Gulley et al., 2009a).

    There exist only a limited number of studies investigating englacial conduit conditions on temperate ice. Studies of glacier's drainage systems are based primarily on dye tracer experiments, speleology, borehole studies, geophysical measurements or

45   a combination of these techniques. Englacial drainage systems have been interpreted from dye testing on temperate glaciers (Nienow et al., 1996, 1998; Hock et al., 1999), but difficulties arose, since tracer tests do not offer direct observations of englacial drainage networks. Direct observations have been made into inactive englacial channels using speleology techniques (Gulley, 2009; Naegeli et al., 2014; Temminghoff et al., 2019), but they were obviously conducted, only when the drainage system was dry and inactive.

50   Geophysical experiments can provide observations on active englacial conduit networks covering a large spatial distribution, and they can be repeated, thereby providing information on the temporal evolution. Ground-penetrating-radar (GPR) has been used to detect englacial drainage systems on cold ice (Moorman and Michel, 2000; Stuart, 2003; Catania et al., 2008; Catania and Neumann, 2010; Schaap et al., 2019; Hansen et al., 2020) and temperate ice (Arcone and Yankielun, 2000; Hart et al., 2015). Across several years, GPR measurements were performed by Bælum and Benn (2011) over a small cold-ice valley

55   glacier to investigate the glacier's thermal regime. Pettersson et al. (2003) used time-lapse GPR, separated by 12 years, to detect changes to the cold-temperate ice transition surface and Irvine-Fynn et al. (2006) used repeated GPR measurements to investigate hydrological seasonal changes on a polythermal glacier. However, for these studies the GPR profiles were not repeated several times during a year and across a number of years. Therefore, very limited information is available on the seasonal evolution of englacial drainage systems on temperate glaciers.

60   In this study, we use a comprehensive GPR dataset that includes annual measurements from 2012, 2016, 2017 and seasonal measurements during 2018 and 2019. This facilitates studying the temporal and spatial changes of an englacial conduit network on a temperate glacier. By repeating GPR measurements several times throughout the melt seasons, we can gain insights into how an englacial network changes and evolves. Additionally, by performing GPR measurements across subsequent melt seasons, we can check, if these englacial networks were reactivated after the winter period in a similar location, or if they close

65   down and become inactive the following melt season. We detect these seasonal and annual changes by extracting the GPR reflection strength (reflectivity) using a GPR impedance inversion scheme (Schmelzbach et al., 2012). The spatial extent of the reflectivity patterns allows potential englacial flow paths to be imaged. In brief, there are three main objectives of this research, namely

1. to implement a GPR processing routine to extract GPR reflection coefficients related to englacial structures,

70   2. to interpret the spatial reflection coefficients in order to gain an understanding of the temporal conduit morphology, and

3. to correlate the englacial conduit's dimensions to previous studies in order to understand the conduit's formation mechanisms.

Furthermore, using a GPR modelling algorithm, we are able to quantify the spatial dimensions of an active englacial conduit network.

75 ## 2 Study Site

This englacial network monitoring case study was conducted on the Rhonegletscher (Fig. 1), where an englacial conduit network was previously detected using active seismic reflection data (Church et al., 2019). The Rhonegletscher is the sixth largest glacier in the Swiss Alps (Farinotti et al., 2009), and it is the source of the Rhone river. The glacier has been well studied and documented due to the ease of access from the nearby Furka pass, with the first measurements from the beginning

80   of the 17th century (Mercanton, 1916). The glacier flows southwards from 3600 down to 2200 m above sea level (asl) with a surface area of approximately 16 km^2 (Huss and Farinotti, 2012). In recent years, a proglacial lake formed as a result of the glacier retreating (Tsutaki et al., 2013; Church et al., 2018). This proglacial lake is dammed by a granite riegel, and there is likely a hydraulic interaction between the lake and the glacier's drainage network. The survey site was located within the lower ablation area between 2280 m and 2350 m asl, where the ice thickness in 2017 was approximately 100 m (Fig. 1).

85 ## 3 Methods

3.1 GPR Data Acquisition

To investigate seasonal englacial conduit variations, we performed several GPR field campaigns from 2012 until 2019 (Table 1). Three GPR surveys, that covered a single profile across the survey site (Q-Q' in Fig. 1), were conducted over three different
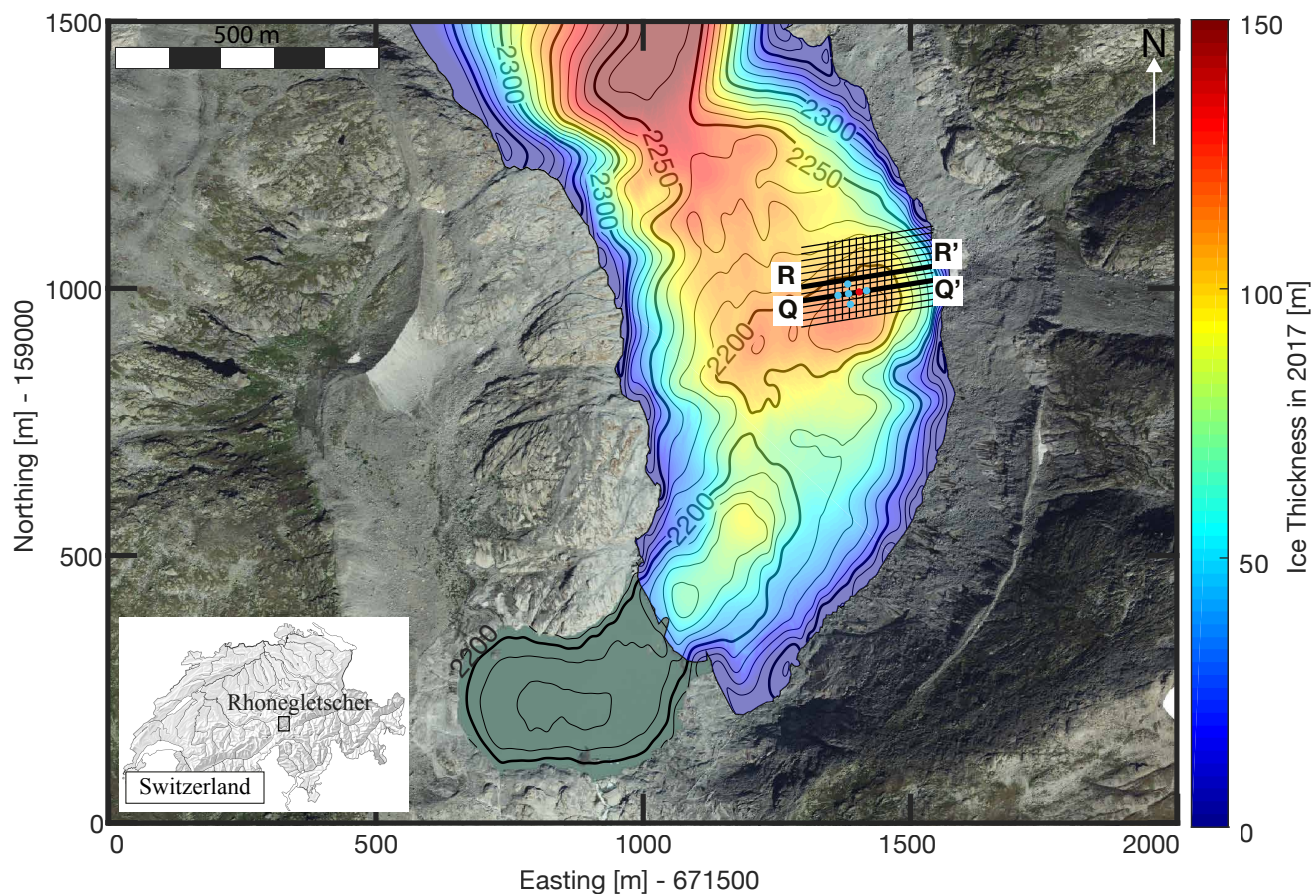
Figure 1. Map of the Rhonegletscher's lower ablation area, ice thickness (colour-coding), basal topography (black contour lines) updated from Church et al. (2018) and GPR repeated survey site (black grid). The two thicker GPR profile lines (R-R' and Q-Q') are displayed in Fig. 3 and Fig. 4. Five boreholes were drilled in August 2018 to provide ground-truths on the conduit and are marked as blue and red dots. The red dot represents the borehole where the borehole camera acquired a video.

years (2012, 2016 and 2017) . Upon detection of the englacial conduit network in 2017 (Church et al., 2019), we performed a
90 dense GPR grid at different times of the year in 2018 and 2019 over the englacial conduit network (grids of black lines in Fig.
1). The GPR grid includes 13 profiles oriented east-west (average length: 250 m) and 10 profiles oriented north-south (average
length: 150 m), with a spacing of 13 m between adjacent profiles.

All field measurements were conducted as common offset (CO) surveys using a Sensor & Software pulseEKKO Pro GPR
system with 25 MHz antennas. The GPR antennas were carried by hand during summer month acquisitions (snow-free, June-
95 October) and during winter month acquisitions (snow covered, November-May), they were mounted and pulled on pulk sleds.
The GPR antennas were positioned in a transverse electric (TE) broadside configuration and kept at a constant offset of
4 m between transmitting and receiving antennas. Additionally, the orientation of the antennas were perpendicular to the

Table 1. Overview of the GPR surveys acquired over the englacial conduit network. Survey months in italic and bold represent winter (snow covered) and summer (snow free) acquisition respectively and the asterisk marks the months where common midpoint measurements were additionally acquired.

Year	No. of surveys	Time of Year	Survey Type
2012	1	**Sep**	Single Profile
2016	1	*Apr*	Single Profile
2017	1	**Sep**	Single Profile
2018	7	*Mar*, *Apr**, *May**, **Jul**, **Sep***, **Oct***, *Dec*	Grid
2019	3	*Feb*, *May*, **Aug**	Grid

walking direction. For all GPR lines, a high precision global navigation satellite system (GNSS) continuously recorded the GPR antennas mid-point and the accuracy given by the GNSS was generally below 0.05 m.

100   In addition to the CO profiles, we acquired common midpoint (CMP) data in order to evaluate the electromagnetic (EM) wave velocity of the glacial ice. These CMP measurements were performed in April, May, September and October 2018 over the englacial conduit in order to detect any seasonal changes to the EM-wave velocities.

3.2   Borehole Data Acquisition

In 2018, six boreholes were drilled around the englacial conduit network (Fig. 1) using a hot water drill. Two boreholes were
105 drilled directly into the conduit network, and we were able to lower a borehole camera (GeoVISION™ Dual-Scan) within these boreholes to make direct observations within the englacial conduit network.

3.3   GPR Data Processing

The raw CO GPR data were processed using a combination of an in-house MATLAB based toolbox (GPRglaz Rutishauser et al. (2016); Langhammer et al. (2017); Grab et al. (2018)) and Seismic Unix. The processing scheme aims to recover the
110 GPR reflection coefficients from the englacial conduit reflections by means of an impedance inversion scheme. This inversion scheme is based upon the seismic impedance inversion developed in the late 1970s and 1980s (Russell, 1988). The reflectivity is recovered by the inversion on pre-conditioned GPR data using the underlying assumption that the GPR reflectivity is represented by a series of sparsely distributed spikes, this inversion is known as a sparse-spiking deconvolution (Velis, 2008). The aim of the sparse-spiking deconvolution operator is to find the smallest number of spikes that, after convolution with the
115 GPR source wavelet, matches the pre-conditioned GPR data within a small error. Within a glaciological setting, the spikes from the deconvolution would represent englacial reflectors or the glacier base. The workflow implemented was based upon the processing described in Schmelzbach et al. (2012).

Table 2. Common offset GPR processing workflow

	Processing Step	Comments
1.	Merge GPR and GNSS data	
2.	Set time zero and record length	2000 ns (~170 m depth of penetration in ice)
3.	Interpolate clipped GPR data	
4.	Butterworth bandpass filter	10-75 MHz
5.	Trace Binning along profile	Binned to 0.5 m spacing
6.	Elevation static correction	
7.	Amplitude corrections	Summer $\alpha = 0.0007$, winter $\alpha = 0.0004$ (see Schmelzbach et al. (2012) for details)
8.	GPR deconvolution	Schmelzbach and Huber (2015)
9.	Phase Shift Migration	Seismic Unix migration and constant velocity of 0.1689 m ns^{-1}
10.	Amplitude matching between all GPR datasets	
11.	Sparse deconvolution to recover reflectivity	Described in Sacchi (1997)
12.	Calibrate the reflectivity	Setting the reflectivity to be the ice-water reflectivity at the borehole site in 2018
13.	Time to depth conversion	Constant velocity 0.1689 m ns^{-1}

An outline of the GPR CO processing is described in Table 2. It consists of the following major steps: (1-6) pre-processing by assigning the GNSS data with the GPR data, setting time zero and the record length, interpolating clipped data, bandpass
120   filtering to remove noise, trace binning to account for varying walking speeds, elevation static correction, (7) deterministic amplitude correction to compensate for the amplitude decay due to gemoetrical spreading, absorption and transmission losses, (8) GPR deconvolution to remove the GPR source wavelet and increase the vertical resolution (Schmelzbach and Huber, 2015), (9) an amplitude preserving migration to re-position the reflections in their correct location and to increase the horizontal resolution, (10) identifying an amplitude matching scalar in order to match the amplitudes across all GPR surveys, (11-13)
125   sparse-spike deconvolution to recover the reflectivity (Sacchi, 1997) and to calibrate the reflectivity and stretch the reflectivity to depth below glacier surface. In order to calibrate the reflectivity, ground truth data were used. The reflectivity within the vicinity of the borehole was calibrated to be the ice-water reflectivity as direct observations provided a flowing water-filled conduit (Church et al., 2019). The outcome of this workflow after migration (9) is shown in Fig. 2 and Fig. 3a-e. The final output (13), including the reflection coefficients, are displayed in Fig. 3f-i.

130   The spatial and temporal distribution of the reflection coefficients is the primary outcome of the processing workflow. The reflection coefficient explains the proportions of energy that are reflected from a given interface. Its values range between -1 and 1. Their magnitudes and polarities are indicative for the electrical material properties adjacent to an interface. Bælum and Benn (2011) divided the zero-offset (vertical incidence) reflection coefficients for glaciological environments into dry and wet groups (Table 3).

Table 3. GPR reflection coefficients from typical glaciological environments using zero-offset measurements (Bælum and Benn, 2011). Wet and dry environments are highlighted by dark grey and light grey cell shading respectively.

		Upper Medium	
		Ice	Water
Lower Medium	Ice	-	+0.67
	Air	+0.28	-
	Granite	-0.11	+0.6
	Wet Sand	-0.47	-
	Water	-0.67	-

135   The GPR reflection coefficient has previously been used in order to determine the presence of water or bed conditions on Matanuska Glacier in Alaska, USA (Arcone et al., 1995). In the Rhonegletscher case study, we will make use of the reflection coefficient for imaging the spatial extent and the temporal evolution of the englacial conduit, and it will also provide information, as to whether the conduit is dry or wet. Since the GPR antennas were constantly separated by 4 m, and the target was around 80-100 m below the glacier surface, the angle of incidence is less than 1 degree, and vertically incident waves can

140   be assumed.

    The CMP measurements were also processed using GPRglaz, but SeisSpace ProMAX 2-D was used for the velocity analysis. The pre-processing included assigning the geometry and amplitude correction for geometrical spreading. As described by Booth et al. (2010), we applied a static shift prior to picking the velocities in ProMAX in order to remove the systematic error in semblance analysis of GPR CMP data. The velocity determined from the CMP measurements (Fig. 4a and d) were used for

145   the migration velocity in the workflow indicated in Table 2.

4   Results

4.1   GPR Imaging Results

For studying the general evolution of the englacial conduit network we analysed all GPR profiles, however we consider profile Q-Q' (Fig. 1) as an example for the annual evolution. In Fig. 2, the GPR sections acquired during the summer' months are

150   displayed. Due to the increased presence of water during the summer melt season, the signature of a potential englacial conduit is expected to be most pronounced during this time of the year. As shown in Fig. 2a, there is no clear englacial reflection visible in September 2012, but in September 2017, we observe a conspicuous reflection pattern at about 2210 m asl (Fig. 2b). This feature is also visible in the GPR sections acquired in summer 2018 and 2019 (Figs. 2c and 2d), although its shape and strengths exhibits some minor variations. From these observations we conclude that this englacial feature is recent, and it must

155   have formed between 2012 and 2017.

Besides the general appearance of this englacial feature, it is also interesting to study its seasonal variability. We analysed all GPR profiles within the grid between 2018 and 2019, however, we consider profile R-R' (Fig. 1) as an example for the seasonal imaging results. In Fig. 3, the GPR sections, acquired in 2018 and 2019, are displayed. Additionally, the spatial distribution of the reflectivity (reflection coefficients) is provided. The single continuous englacial reflector is present across the majority of

160 the acquired profile during the summer months (Fig. 3c and e), whereas in April 2018 (winter) it is almost absent (Fig. 3b), and its reflection strength is also reduced in May 2019 (winter) (Fig. 3d). The reflectivity (Fig. 3f-i) emphasises the contrasting englacial environment between summer and winter. Similar observations were also made in profile Q-Q' (not shown) and across the majority of GPR profiles acquired, but in profile R-R' they are slightly more pronounced.

4.2 GPR Common Midpoint Results

165 The CMPs were acquired in order to determine the EM wave propagation velocity through glacial ice for the CO phase shift migrations and to determine, if any seasonal variation exist. Four CMPs were acquired at different times of the year (Table 1), and the velocities were picked using semblance analysis from SeisSpace ProMAX 2-D. The location of the CMPs was directly over the englacial conduit (marked by the green line in Fig. 2c), where the conduit was a specular reflector showing little topography variation. Furthermore, prior to picking the velocities, the CMPs were backshifted by a quarter wavelength,

170 as suggested by Booth et al. (2010).

The velocities were picked on the englacial reflection using a second order normal moveout correction. The EM wave propagation velocity for the winter CMP measurement (Fig. 4a) was picked on the semblance to be between 0.16 and 0.17 m ns^{-1} (Fig. 4b-c). The EM wave propagation velocity during the summer CMP measurement (October 2019) was between 0.165 and 0.175 m ns^{-1}. There exist some uncertainty as a result of limited transmitter-receiver offsets in comparison to the

175 target depth (offset-depth ratio: 0.5), and the low frequency antenna with a dominant period of 15 ns create large semblance bullseyes in Figs. 4c and f. Two more CMP gathers were recorded in May and September 2019, which show a similar velocity, but with a larger uncertainty due to poorer data quality.

The EM wave propagation velocities within ice is a function of water content, and quoted values in literature are between 0.167 and 0.169 m ns^{-1} (Fujita et al., 2000; Murray et al., 2000; Plewes and Hubbard, 2001; Reynolds, 2011; Bradford et al.,

180 2013). As a result of the uncertainties on the propagation velocities from the CMP measurements, the migration velocity was kept constant for both summer and winter at 0.169 m ns^{-1} as used in previous temperate ice GPR studies (Glen and Paren, 1975; Rutishauser et al., 2016).

4.3 GPR Seasonal Reflectivity Results

The reflectivity from the top of the englacial reflection was extracted (red arrows highlighting the negative reflectivity event in

185 Fig. 3g), interpolated and smoothed for each seasonal GPR acquisition over the survey area. Figure 5 highlights the seasonal spatial reflectivity over 16 months from May 2018 until August 2019. The white lines in Fig. 5 correspond to isolines with reflectivity of -0.11, which correlates to the boundary between dry and wet glacial reflection environments (Table 3). During the
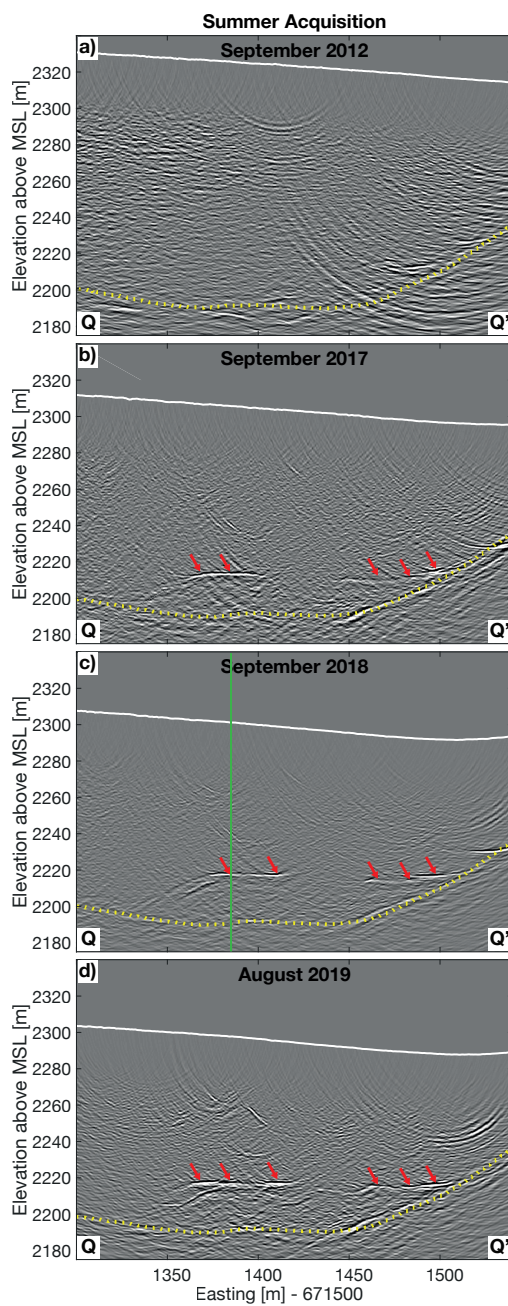
Figure 2. GPR imaging results from a repeated profile (Q-Q' in Fig. 1) over a single line after migration from 2012 until 2019. The yellow line represents the ice-bedrock interface and the red arrows represent the englacial conduit network reflection appearing from summer 2017. The green line in c) marks the location of the CMP acquired

f
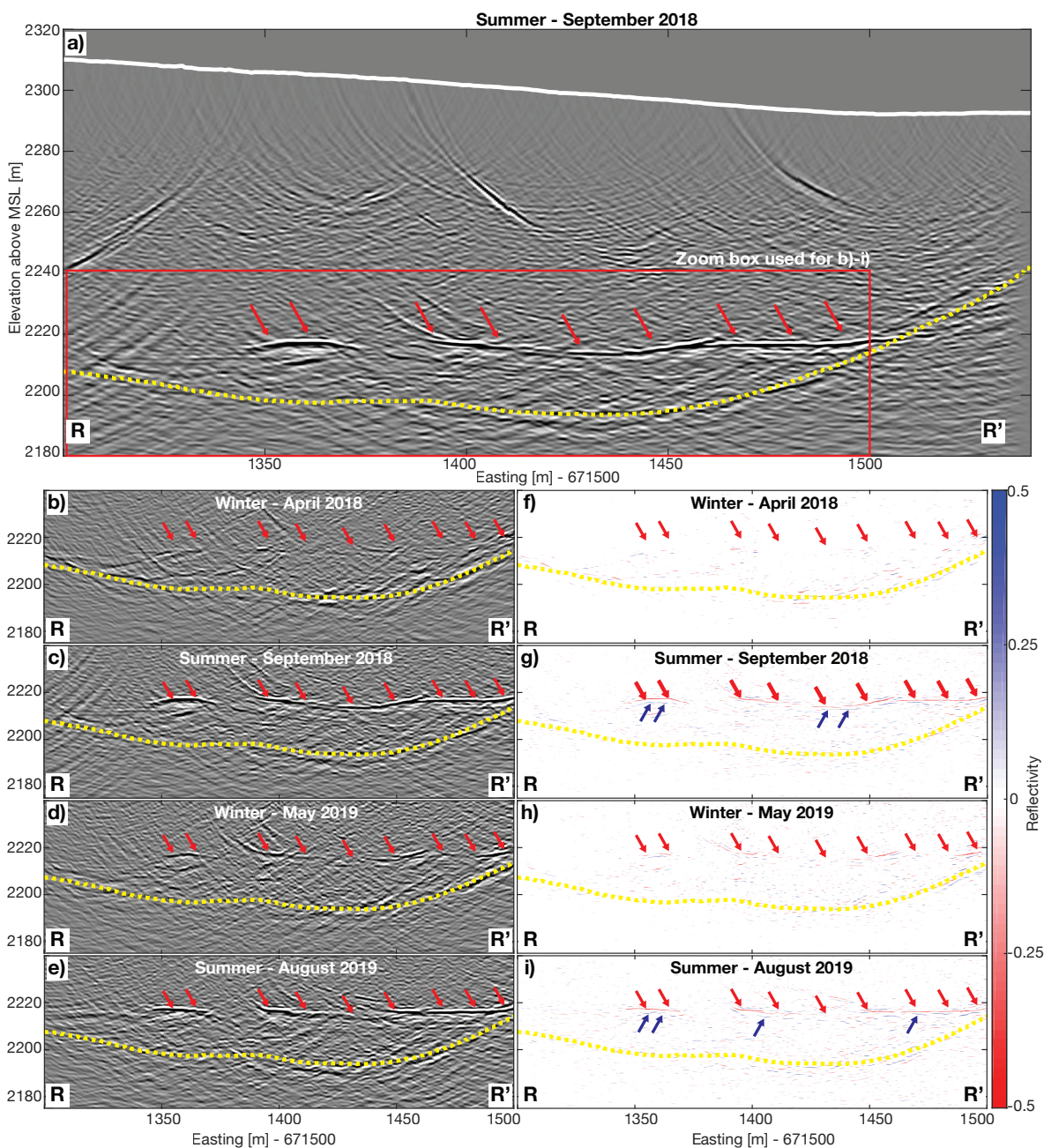
Figure 3. a) GPR imaging results over a single repeated GPR profile (R-R' in Fig. 1) in 2018. The yellow line represents the ice-bedrock interface, white line represents the glacier surface, and the red box is the zoom box for GPR imaging and reflectivity results b)-i). b)-e) are seasonal GPR imaging results and f)-i) are the seasonal GPR reflectivity results from b)-e). The red arrows represent the top of the englacial conduit network and the blue arrows represent the bottom of the englacial conduit network (g & i).
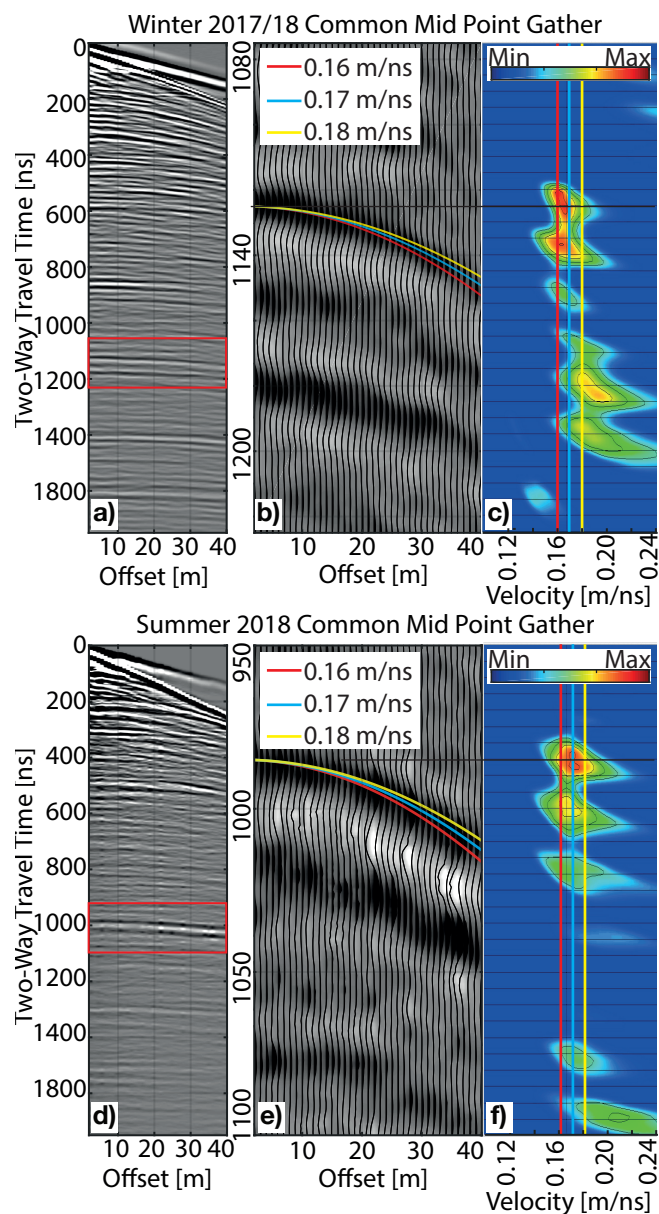
Figure 4. Common mid point gather and velocity determination. Winter (April 2018): a) The raw CMP gather. b) Zoom of the raw gather over the englacial reflection with second order normal moveout (NMO) curves using 0.16, 0.17 and 0.18 m ns^{-1}. c) Semblance display using second order NMO for the zoom section from b). Summer (October 2018): d)-f) as per winter a)-c).

summer months, when the englacial conduit is active and transporting melt water through the glacier's body we observe large negative reflectivities (<-0.2). The spatial extent of the englacial network is clearly visible in the summer months acquisition.
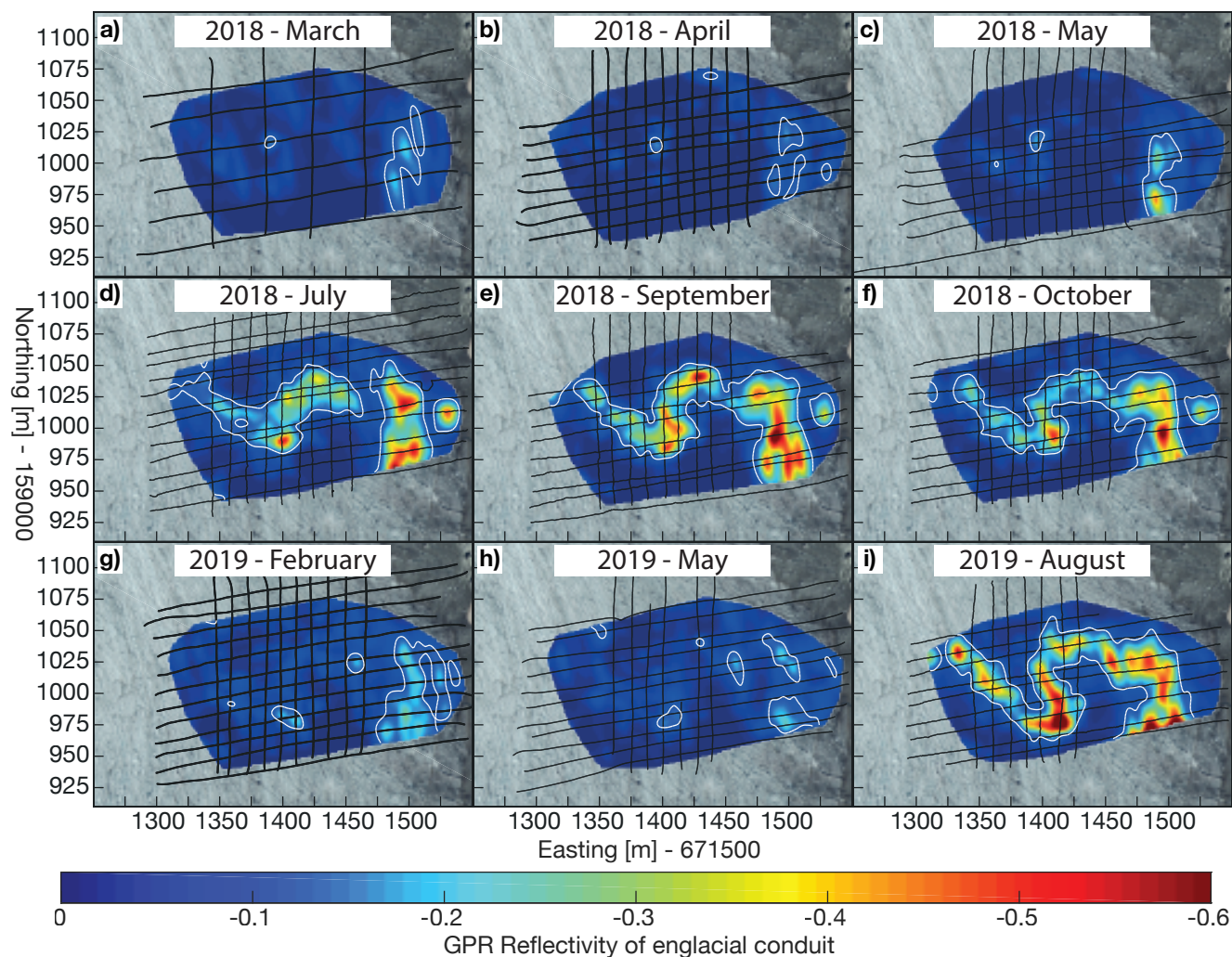
Figure 5. Seasonal GPR reflectivity from the top of the englacial channel reflection. The black grid lines represent the GPR acquisition profiles acquired for each month respectively. The white contour represents the reflectivity at -0.11.

190   The reflectivity during the winter months (Fig. 5a-c & g-h) is around zero indicating that the channel is not a wet environment. Whereas, during the summer months (Fig. 5d-f & i) the reflectivity varies between -0.2 and -0.6, corresponding to the wet reflectivity scenarios in Table 3. At the beginning of the melt season in July 2018 (Fig. 5d), the englacial conduit network does not appear to be fully developed and connected throughout the survey site, while in September and October 2018 (Fig. 5e & f), the conduit is connected across the survey site. Furthermore, in August 2019 (Fig. 5i), we observe wet-environment

195   reflectivities in an identical location as in summer 2018.

4.4 GPR Conduit Thickness Results

In addition to the seasonal reflectivity results, the conduit thickness was calculated for those surveys, where top and bottom reflections could be identified clearly. The travel time differences between the top and bottom reflections was converted to thickness using the velocity of an EM wave travelling through water (0.0333 m ns^{-1}). Figure 3g and i shows a negative

200 reflectivity for the top of the conduit (red arrows) and a positive reflectivity for the bottom of the conduit (blue arrows). Upon extraction of the conduit thickness, the spatial extent of the conduit thickness was determined by interpolating between the GPR profiles and smoothing (Fig. 6). The conduit thickness is between 0.2 and 0.5 m throughout the melt season (Fig. 6), and there is little variability in the conduit thickness throughout the summer.

Reynolds (2011) states that, in theory, the vertical resolution of a GPR signal is a quarter wavelength, assuming the source

205 wavelet is two half cycles. This theory is based upon the seismic wave propagation theory as described by Widess (1973). In reality the GPR source wavelet is typically longer than a single wavelength, with this being the case, the vertical resolution is reduced as a result of the complex nature of the transmitted GPR source wavelet (Reynolds, 2011). For an EM wave propagating within a water-filled conduit the wavelength of a 25 MHz system is 1.333 m, and therefore the theoretical vertical resolution ($\lambda/4$) for a conduit filled with water using 25 MHz antennas is 0.33 m. The true conduit thickness can be determined from

210 the reflectivity inversion if the thickness of the conduit is larger than the theoretical vertical resolution. The thicknesses shown in Fig. 5 are thus within proximity of the theoretical vertical resolution limit. Therefore, we performed a thin-layer forward modelling investigation, with which we tried to appraise the reliability and robustness of the thickness estimates.

4.5 Thin Channel Water Layer GPR Forward Modelling Results

A forward modelling approach was adopted in order to investigate how a thin water filled channel layer, below the theoretical

215 vertical resolution, affects the observed thickness and reflectivity that we recover from the processing workflow described in Table 2. We generated synthetic radargrams using the open source software gprMax (Warren et al., 2016). This is a finite-difference time-domain solver for EM wave propagation. We employed a simple 3D model, as sketched in Fig. 7a. It includes a single thin water filled conduit that is invariable in the third dimension. The associated material parameters are summarised in Table 4. All four boundaries of the model had absorbing boundary conditions in order to prevent multiple energy interfering

220 with the top and bottom reflection from the conduit. The synthetic GPR data (Fig. 7b) were modelled using transmitting and receiving antennas separated by 2 m, and they were moved from 2 until 18 m along the x axis in Fig. 7a at 0.5 m increments. The model space did not contain a free surface in order to have a clear interpretation of the top and bottom conduit reflector without any multiple energy being present.

The synthetic GPR data, shown in Fig. 7b, were generated with a 2 m thick water-filled englacial conduit, and the red and

225 blue arrows represent the reflection from the top and bottom conduit respectively. There is clear separation between the top and bottom reflections from the conduit using a 2 m thick englacial conduit model, but, as shown in Figure 8, these two reflectors interfere with each other, when the conduit thickness reaches the vertical resolution (0.3 m in Fig. 8). The horizontal width of the water-filled conduit remained at 5 m for all tests and is below the horizontal resolution after migration. In order to
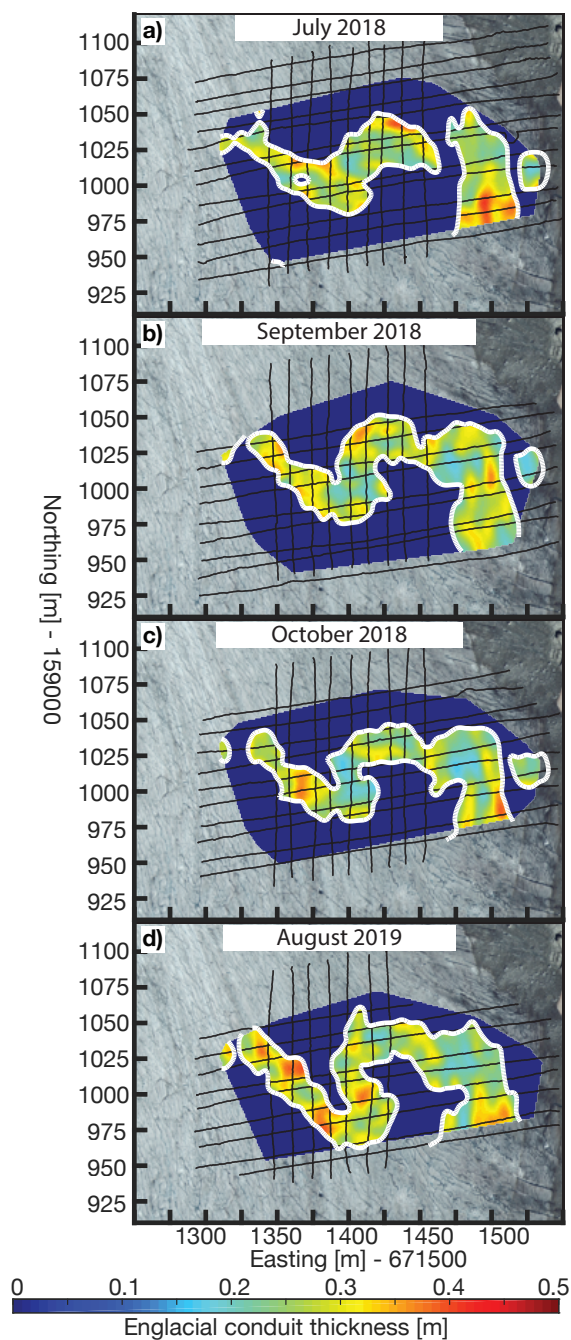
Figure 6. Estimated englacial conduit thickness during the summer months of (a-c) 2018 and (d) 2019. The white contour represents the englacial conduit reflectivity at 0.1, same contour as displayed in Fig. 5.
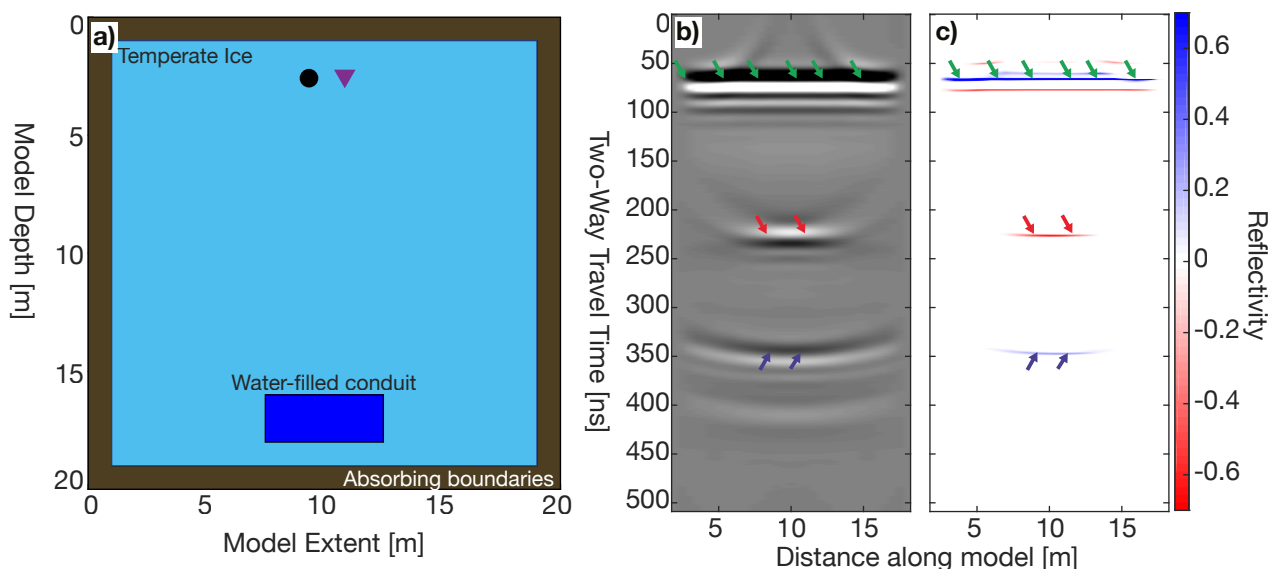
Figure 7. Forward modelling results. a) Geometry model for gprMax forward modelling with temperate ice, 2 m thick water-filled conduit and absorbing boundaries labelled. The circle and the triangle represent the transmitting and receiving antenna. b) The processed synthetic data generated from the model in a) after step 10 in Table 2. c) The reflectivity from the data b) after processing through the entire workflow described in Table 2. The green arrows represent the direct arrival, the red and blue represent the top and bottom reflection from the englacial conduit respectively.

extract the reflectivity (Fig. 7c and Fig. 8b) from the synthetic GPR data, the data were processed using an identical processing

230 workflow, as applied to the field data.

The numerical simulations and thickness extraction procedures were repeated with a range of conduit thicknesses between 0.05 and 2 m. The results are shown in Fig. 9a. We were able to determine the correct conduit thickness, when the true thickness was greater than 0.4 m (0.3λ). However, when a water filled conduit was less than 0.4 m thick, the observed thickness from the inversion was within ± 0.15 m (yellow shaded area in Fig. 9a). In the summer, the majority of the Rhonegletscher imaged

235 englacial conduit network is less than 0.4 m (Fig. 6) and therefore, the conduit thickness does not represent the true thickness but the calculated thickness is within ± 0.15 m of the actual conduit thickness.

In addition to the discrepancies between observed channel thickness and true channel thickness (Fig. 9a), the GPR zero-offset reflectivity can be analysed as a function of channel thickness (Fig. 9b). In order for the channel to have an ice-water reflectivity of -0.67 (Table 3) the conduit must be greater than 0.6 m thick (0.45λ), as represented by the green shaded area

240 in Fig. 9b. When the conduit is between 0.1 and 0.6 m thick (0.07λ - 0.45λ), the calculated reflectivity is equal to the true reflectivity ± 0.1 (shaded yellow area in Fig. 9b). When the conduit is thinner than 0.1 m, the calculated reflectivity is below 0.5 (shaded red area in Fig. 9b). From these results, a likely explanation for the low reflectivities observed from the conduit (Fig. 5) could be the result of the conduit being below the vertical resolution.
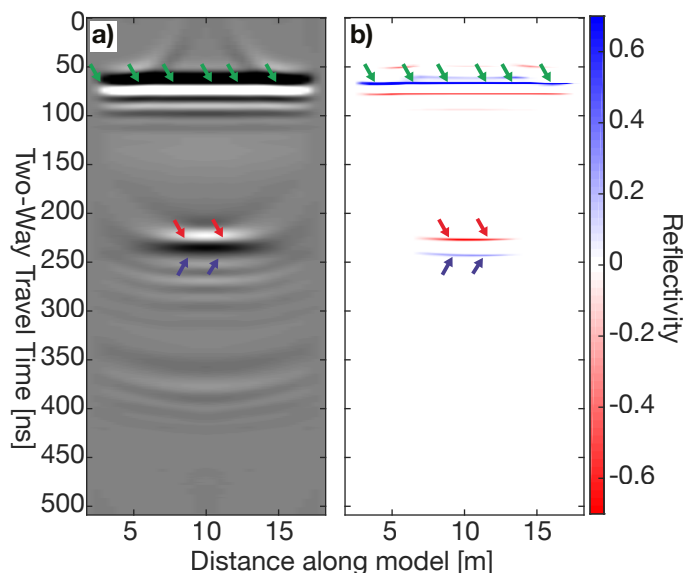
Figure 8. Forward modelling results for 0.3 m water-filled conduit. a) The processed synthetic data after step 10 in Table 2. c) The reflectivity from the data a) after processing through the entire workflow described in Table 2. The green arrows represent the direct arrival, the red and blue represent the interfering top and bottom reflection from the englacial conduit respectively.

Table 4. Material properties for the forward modelling, taken from (Plewes and Hubbard, 2001; Reynolds, 2011; Langhammer et al., 2017)

Material	Relative permittivity ϵ	Conductivity σ [S/m]	Relative permeability μ	Magnetic Loss [Ω/m] σ	Velocity [m/ns]
Temperate ice	3.2	$5e^{-8}$	1	0	0.1689
Fresh water	80	0.0005	1	0	0.033

5 Discussion

5.1 Conduit Extension

During the melt season (July-October), when the englacial conduit is active, the conduit is around 250 m in length and between 20-45 m wide. During all the summer acquisitions, the englacial conduit thickness was estimated to be between 0.2 and 0.4 m exhibiting little variability (Fig. 6). Therefore, the conduit was far wider than thick and it does not follow the typical cylindrical englacial conduit cross-sectional shape, as observed in other GPR surveys (Stuart, 2003), or as described by theory (Shreve, 1972; Roethlisberger, 1972).
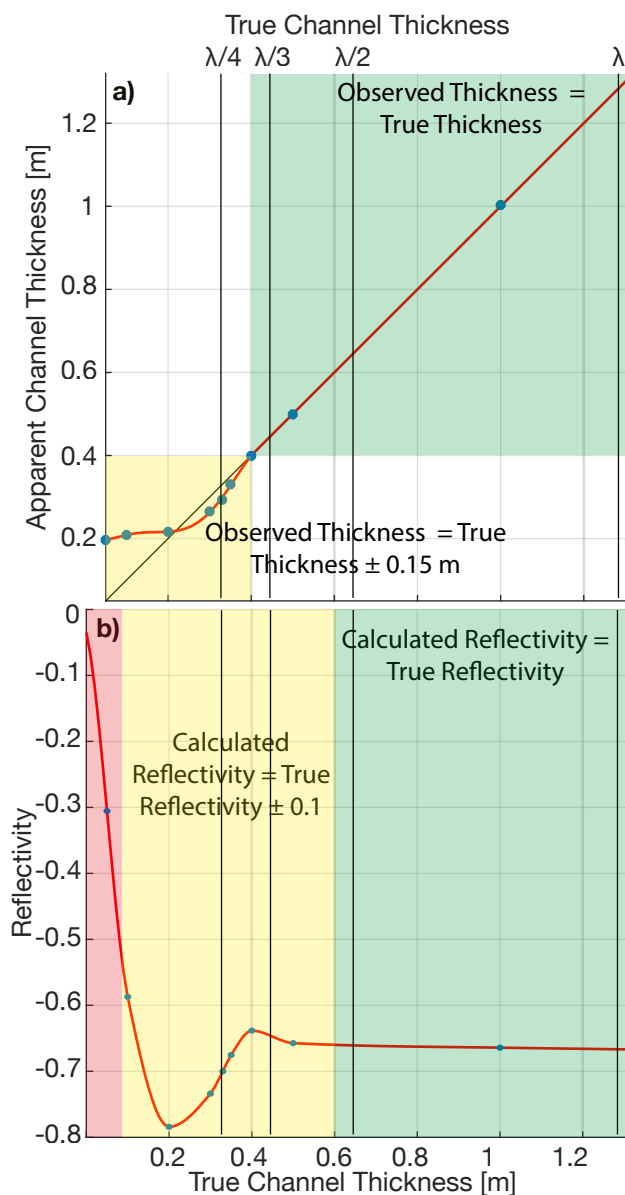
Figure 9. Forward modelling thickness and reflectivity results plotted against model conduit thickness. a) The observed thickness in the GPR inversion processing as a function of the true channel thickness in the model (Fig. 7a using 25 MHz antennas). b) The calculated reflectivity from the channel top as a function of the true channel thickness.

5.2 Conduit Inclination

There is a ten metre elevation difference in the conduit's topography (Fig. 10) across the entire imaged englacial conduit network, thereby indicating that the conduit has a low inclination (approximately 2°). It is similar to englacial conduits drainage networks found on a cold-ice glacier in Svalbard (Stuart, 2003; Hansen et al., 2020). Such a small dip provides evidence that the

255   movement of englacial water is not related with the hydraulic gradients and therefore, does not supports the englacial conduit formation models described by Shreve (1972), which postulates englacial conduits formation through upward branching of an arborescent network.

5.3 Conduit Shape

The shape of the englacial conduit shows a sinusoidal outline that runs perpendicular to the ice flow direction. The outline

260   (white contour in Fig. 6) has similar geometry to sub-sections of englacial conduits that have been mapped using speleology within cold glaciers (Gulley et al., 2009a), which have been formed as a result of the cut-and-closure mechanism. Similarly, a sinusoidal shape could result from turbulent water flowing englacially. To the best of our knowledge this is the first example of a temperate glacier to have an active englacial system surveyed using geophysical techniques and showing a sinusoidal shape.

5.4 Conduit Formation

265   The conduit's sinusoidal shape provides some evidence that this englacial drainage system could be the result of a cut-and-closure drainage system. However this hypothesis can be ruled out, as no large visible supraglacial stream has been observed on Rhonegletscher within the proximity of the englacial conduit in previous years. Moreover, comparing the conduit's profile and cross sections with those described by Gulley et al. (2009a) and summarised in Fig. 2 in their publication, the likely formation mechanism is extensional hydrofracturing. Hydrofracturing on extensional stressed glacial ice provides a horizontal

270   profile (shallow dip) and an englacial conduit cross-section that is thin and wide. Such extensional stresses may result from the turning of the Rhonegletscher at the survey site towards the proglacial lake. As discussed in Church et al. (2019), the drainage network is likely fed from numerous streams running along the glacier margin and from the surrounding moraine. Additionally, the hydrofracturing can be supported by the fact that periods of high water pressure was observed as a result of the borehole expelling water 3-4 m above the glacier surface in August 2018.

275   We were unable to determine the flow direction from either the GPR data or from the borehole camera. Tracer studies might be an option (Hooke and Pohjola, 1994; Hock et al., 1999). Unfortunately, this would be difficult, as the studied englacial network is expected to flow into the proglacial lake, and therefore monitoring the tracer quantity would require samples to be taken directly from a borehole instead of an outflow stream from the glacier's tongue.

5.5 Conduit's Seasonal Variations

280   The conduit morphology alters throughout the year as a result of the varying discharge from the glacier. For a steady-state englacial conduit, where the conduits opening rates equals the conduits closure rate, the size and shape of the conduit re-
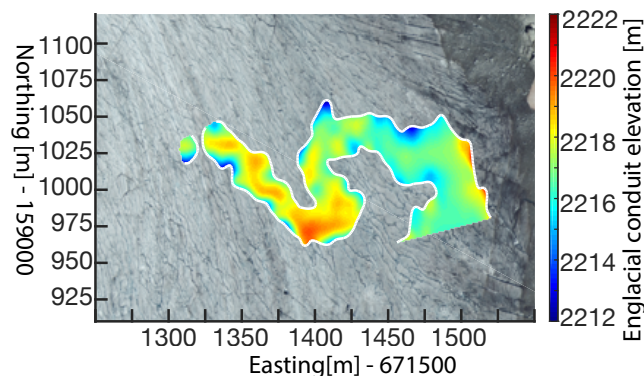
Figure 10. Elevation above mean sea level from the top of the englacial conduit network in August 2019.

mains constant. Changes in water supply can alter the opening and closure rates and thereby alter the conduit's morphology. Englacial conduits can shrink and disappear, when discharge quantities are low, whereas high discharge rates can cause a conduit to expand. Runoff and discharge data are available at a gauging station in Gletsch (1800 m a.s.l), 2 km downstream from Rhonegletscher. The peak discharge occurs annually between 24th July and 17th August. The end of the peak discharge correlates with the time of the year, where the conduit was well developed in 2019 (Fig. 6d). We can speculate that during August, when there are exist a large diurnal discharge fluctuations through the englacial conduit, the englacial network is fully developed. The timing further correlates with observations from other alpine glaciers, where subglacial drainage networks often switch from a distributed system to a channelised system in the peak of the melt season (Seaberg et al., 1988; Nienow et al., 1996).

There exists a winter shut-down of the englacial conduit network between 2018 and 2019, indicated by a near-zero reflectivity (Fig. 5e). Remnants of the englacial conduit is detectable on the winter reflectivity, when restricting the colour scale from -0.05 to -0.15 (Fig. 11, grey line). If the conduit is fully open (thickness > 0.5 m), then it is neither water or air filled during the winter as a large negative reflectivity (ice-water: -0.67) or positive reflectivity (ice-air: +0.3) is not observed. During August 2018, we were able to make direct borehole measurements using a borehole camera and observed sediment being transported along the base of the conduit (see video supplement). Therefore, as a result of the lower reflectivity and the lower discharge, we speculate that during winter the conduit either physically closes or becomes very thin (< 0.1 m) and remains water filled. If the conduit physically closes, the sediments lying within the closed conduit are likely the cause of the low winter reflectivity, and the reflectivity values around -0.1 indicate a dry glacial environment (Table 3). Whereas, if the conduit thinned to less than 0.1 m and remained water filled the reflectivity values are around -0.1 (red area in Fig. 9b). The repeated GPR summer measurements in 2018 and 2019 provided evidence that the conduit networks reopens in an identical location. In order for the conduit to be reactivated during the 2019 melt season, either the sediments lying within the closed during the winter months provided a potential permeable flow path in 2019, or the englacial conduit remained connected after becoming a very thin
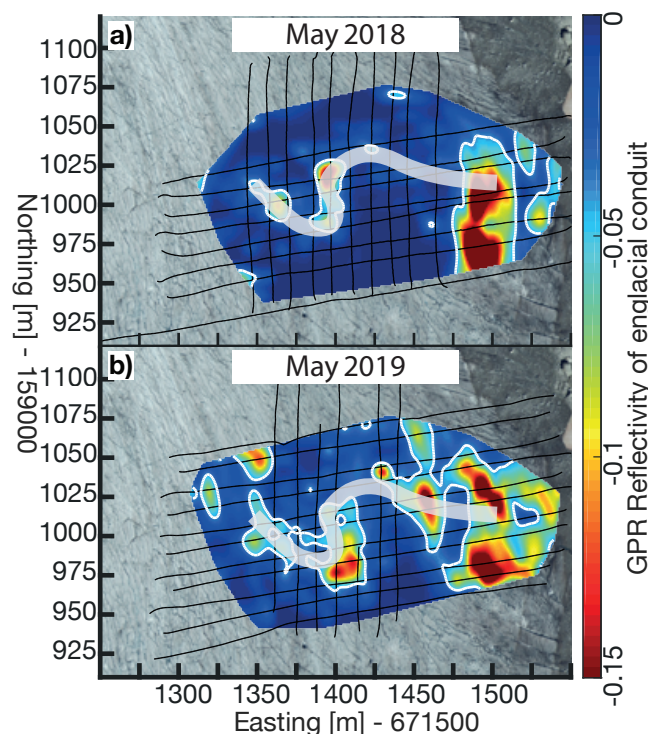
Figure 11. Winter GPR reflectivity from the top of the englacial channel reflection plotted between 0 and -0.15 reflectivity values, highlighting remnants of the englacial conduit network that exist during the winter months. The grey line represents the summer englacial conduit shape. The black grid lines represent the GPR acquisition profiles acquired for each month respectively. The white contour represents the reflectivity at -0.05.

water-filled (<0.1 m) conduit during the winter. Furthermore, we speculate that the hydraulic potential is similar during both

305   melt seasons as the englacial conduit is reactivated in an identical position after the winter shutdown.

The GPR wavelet character from the conduit's top remains a constant negative high amplitude reflector over the three melt season (2017, 2018 and 2019), which indicates the presence of water within the system during our GPR summer acquisitions. From the GPR data, we are able to determine that the englacial conduit network is at or above atmospheric pressure. If the system would be below atmospheric pressure, the top reflector would be an interface between ice and air and result in a positive

310   amplitude reflector. Such an unpressurised englacial network was observed by Stuart (2003), where the conduit's top reflection was a high positive amplitude reflector. The fact that the conduit is at or above atmospheric pressure is additionally supported by our borehole camera observations, where the borehole water level that was 1-2 m above the englacial network during observations, suggesting that the water pressure was slightly above atmospheric pressure.

5.6 General Applicability and Limitations of GPR to Characterise Englacial Conduits

315 So far, there exist a few studies, where englacial conduits have been characterised using a combination of GPR with speleology or borehole observations (Moorman and Michel, 2000; Stuart, 2003; Catania et al., 2008; Temminghoff et al., 2019; Schaap et al., 2019). In these studies, englacial conduits were imaged as point diffractors. Without speleology or boreholes, the interpretation of these point diffractors is typically ambiguous. In the Rhonegletscher case study, the interpretation is unambiguous with the ground-truth borehole observations, because the englacial conduit appears a single specular reflection.

320 For future studies investigating englacial conduits, the GPR reflectivity workflow can be used to identify englacial conduits and conditions on the glacier's bed, but it is essential to calibrate the observed reflectivities with known reflectivities on site. For the Rhonegletscher data, this was obtained from borehole observations. However, for others studies, a known reflectivity point may not be available in order to calibrate the reflectivity, and therefore by plotting the uncalibrated reflectivity of an englacial reflector potential flow paths could be delineated, however the filling material would remain unknown. Such an approach

325 was adopted in Bælum and Benn (2011) (plotting the reflection normalised amplitude of the glacier's bed). The workflow could be extended to specular glacier basement reflectors in order to detect subglacial conduit networks. However, the GPR processing workflow does not correct for the anisotropic GPR radiation pattern. In this case, dipping specular reflectors will have amplitudes dependent on both the radiation pattern and the angle dependent reflection coefficient. Therefore an extension of the workflow needs to be made and a migration accounting for GPR antenna radiation pattern needs to be implemented prior

330 to the impedance inversion in order to extract the reflectivity coefficient.

This study has also provided evidence that the glacier's bed needs to be interpreted with care. The Rhonegletscher case study has identified an englacial conduit as a specular reflector 10-15 m above the glacier's bed during the melt season. If a single GPR profile would have been acquired during the melt season (e.g. August 2019, Fig. 3e), the englacial conduit may have been mis-interpreted as the glacier bed. Therefore, it is essential to understand the hydrological conditions of the glacier,

335 when designing GPR surveys in order to successfully interpret the GPR data. For GPR surveys, where the ice thickness is the objective on temperate alpine glaciers, then GPR acquisition should be undertaken during winter in order to minimise the englacial water storage limiting penetration depth. On the contrary, for GPR surveys investigating the glacier's hydrological conditions it is intuitive that acquisition should take place during summer.

From the forward modelling, the vertical resolution for GPR was found to be 0.3λ. If two interfaces are spaced less than

340 $0.3\ \lambda$ metres vertically apart, then there exists interference between the two reflectors which leads to an erroneous thickness interpretation (Fig. 9). This GPR vertical resolution is larger than seismic vertical resolution found through forward modelling on ice-water reflectivities (King et al., 2004), as a result of the complex nature of the GPR source wavelet.

6 Conclusions

By using repeated GPR measurements and processing the data with an impedance inversion to extract the reflectivity, we have

345 mapped the changing spatial extent and thickness of an active and dynamic englacial conduit network on a temperate glacier.
The repeated seasonal GPR measurements in 2018 and 2019 and the reflection coefficient analysis of the englacial conduit provided an insight into the evolution of an active englacial hydrological network.

In summer the englacial conduit was active, leading to large negative reflectivity values (<-0.2). The Rhonegletscher's englacial network followed a sinusoidal shape throughout the melt season. The conduit is 15-20 m wide and between 0.2 and

350 0.4 m thick. Such a conduit cross section (wide and thin) can occur as a result of hydraulic fracturing with extensional stresses acting on the ice, based upon the englacial conduit shape review by Gulley et al. (2009a). Furthermore, water flowing through the englacial conduit during the melt season feeds the subglacial drainage network, which likely increases subglacial water pressure and facilitates basal sliding.

The englacial conduit was found to be inactive during the winter period, with reflectivity values between -0.05 and -0.15.

355 Therefore, we speculate that during the winter the conduit network either physically closes or is very thin (<0.1 m). Either, sediments that were being transported within the conduit in the summer or water within a thin-layer conduit are likely responsible for the reflectivity visible during the winter GPR acquisition. The englacial conduit became active in an identical location after a winter shut down. The conduit's shape remained similar in the winter compared to the summer.

Difficulties arise when interpreting a series of reflectors that are separated by the vertical resolution. The forward modelling

360 has shown that two horizons are perfectly distinguishable when they are separated by more than 0.3λ. Whereas, the amplitude or reflectivity of the top interface is only resolved when the thickness is greater than 0.45λ. We conclude that care must be taken when inferring material properties from a reflectivity processing workflow with the presence of thin layers that approach the vertical resolution of the GPR source wavelet.

Video supplement. Movie S1 https://doi.org/10.3929/ethz-b-000406689 shows the borehole camera observations made directly into the ac-

365 tive englacial conduit on 24th July 2018.

Author contributions. GC, MG, AB and HM designed the GPR experiments, which were carried out by GC and MG. GC processed the data with help from CS and all authors analysed the data. GC interpreted the data with help from all co-authors. GC wrote the manuscript with contributions from all co-authors.

Competing interests. The authors declare that they have no conflict of interest.

370 *Acknowledgements.* The Swiss National Science Foundation financed the project (SNF Grant 200021_169329/1). Data acquisition has been provided by the Exploration and Environment Geophysics (EEG) group and the Laboratory of Hydraulics, Hydrology and Glaciology (VAW) of ETH Zurich. The authors gratefully acknowledge the Landmark Graphics Corporation for providing data processing software through the Landmark University Grant Program. The authors wish to acknowledge all volunteers for their valuable help in participating the fieldwork.

References

375   Arcone, S. A. and Yankielun, N. E.: 1.4 GHz radar penetration and evidence of drainage structures in temperate ice: Black Rapids Glacier, Alaska, U.S.A., Journal of Glaciology, 46, 477–490, https://doi.org/10.3189/172756500781833133, 2000.

Arcone, S. A., Lawson, D. E., and Delaney, A. J.: Short-pulse radar wavelet recovery and resolution of dielectric contrasts within englacial and basal ice of Matanuska Glacier, Alaska, U.S.A., Journal of Glaciology, 41, 68–86, https://doi.org/10.1017/S0022143000017779, 1995.

Bælum, K. and Benn, D. I.: Thermal structure and drainage system of a small valley glacier (Tellbreen, Svalbard), investigated by ground
380   penetrating radar, The Cryosphere, 5, 139–149, https://doi.org/10.5194/tc-5-139-2011, 2011.

Benn, D., Gulley, J., Luckman, A., Adamek, A., and Glowacki, P. S.: Englacial drainage systems formed by hydrologically driven crevasse propagation, Journal of Glaciology, 55, 513–523, https://doi.org/10.3189/002214309788816669, 2009.

Bingham, R. G., Nienow, P. W., Sharp, M. J., and Boon, S.: Subglacial drainage processes at a High Arctic polythermal valley glacier, Journal of Glaciology, 51, 15–24, https://doi.org/10.3189/172756505781829520, 2005.

385   Bingham, R. G., Hubbard, A. L., Nienow, P. W., and Sharp, M. J.: An investigation into the mechanisms controlling seasonal speedup events at a High Arctic glacier, Journal of Geophysical Research: Earth Surface, 113, 1–13, https://doi.org/10.1029/2007JF000832, 2008.

Boon, S. and Sharp, M.: The role of hydrologically-driven ice fracture in drainage system evolution on an Arctic glacier, Geophysical Research Letters, 30, 3–6, https://doi.org/10.1029/2003GL018034, 2003.

Booth, A. D., Clark, R., and Murray, T.: Semblance response to a ground-penetrating radar wavelet and resulting errors in velocity analysis,
390   Near Surface Geophysics, 8, 235–246, https://doi.org/10.3997/1873-0604.2010008, 2010.

Bradford, J. H., Nichols, J., Harper, J. T., and Meierbachtol, T.: Compressional and EM wave velocity anisotropy in a temperate glacier due to basal crevasses, and implications for water content estimation, Annals of Glaciology, 54, 168–178, https://doi.org/10.3189/2013AoG64A206, 2013.

Catania, G. A. and Neumann, T. A.: Persistent englacial drainage features in the Greenland Ice Sheet, Geophysical Research Letters, 37, 1–5,
395   https://doi.org/10.1029/2009GL041108, 2010.

Catania, G. A., Neumann, T. A., and Price, S. F.: Characterizing englacial drainage in the ablation zone of the Greenland ice sheet, Journal of Glaciology, 54, 567–578, https://doi.org/10.3189/002214308786570854, 2008.

Church, G., Bauder, A., Grab, M., Rabenstein, L., Singh, S., and Maurer, H.: Detecting and characterising an englacial conduit network within a temperate Swiss glacier using active seismic, ground penetrating radar and borehole analysis, Annals of Glaciology, 60, 193–205,
400   https://doi.org/10.1017/aog.2019.19, 2019.

Church, G. J., Bauder, A., Grab, M., Hellmann, S., and Maurer, H.: High-resolution helicopter-borne ground penetrating radar survey to determine glacier base topography and the outlook of a proglacial lake, in: 2018 17th International Conference on Ground Penetrating Radar (GPR), pp. 1–4, IEEE, https://doi.org/10.1109/ICGPR.2018.8441598, 2018.

Cuffey, K. M. and Paterson, W. S. B.: The Physics of Glaciers, Fourth Edition, Academic Press, fourth edi edn., 2010.

405   Farinotti, D., Huss, M., Bauder, A., and Funk, M.: An estimate of the glacier ice volume in the Swiss Alps, Global and Planetary Change, 68, 225–231, https://doi.org/10.1016/j.gloplacha.2009.05.004, 2009.

Fountain, A. G. and Walder, J. S.: Water flow through temperate glaciers, Reviews of Geophysics, 36, 299–328, https://doi.org/10.1029/97RG03579, 1998.

Fountain, A. G., Jacobel, R. W., Schlichting, R., and Jansson, P.: Fractures as the main pathways of water flow in temperate glaciers, Nature,
410   433, 618–621, https://doi.org/10.1038/nature03296, 2005.

Fujita, S., Matsuoka, T., Ishida, T., Matsuoka, K., and Mae, S.: A summary of the complex dielectric permittivity of ice in the megahertz range and its applications for radar sounding of polar ice sheets, Physics of Ice Core Records, pp. 185–212, 2000.

Glen, J. W. and Paren, J. G.: The Electrical Properties of Snow and Ice, Journal of Glaciology, 15, 15–38, https://doi.org/10.3189/S0022143000034249, 1975.

415   Grab, M., Bauder, A., Ammann, F., Langhammer, L., Hellmann, S., Church, G., Schmid, L., Rabenstein, L., and Maurer, H.: Ice volume estimates of Swiss glaciers using helicopter-borne GPR an example from the Glacier de la Plaine Morte, in: 2018 17th International Conference on Ground Penetrating Radar (GPR), pp. 1–4, IEEE, https://doi.org/10.1109/ICGPR.2018.8441613, 2018.

Gulley, J.: Structural control of englacial conduits in the temperate Matanuska Glacier, Alaska, USA, Journal of Glaciology, 55, 681–690, https://doi.org/10.3189/002214309789470860, 2009.

420   Gulley, J., Benn, D., Müller, D., and Luckman, A.: A cut-and-closure origin for englacial conduits in uncrevassed regions of polythermal glaciers, Journal of Glaciology, 55, 66–80, https://doi.org/10.3189/002214309788608930, 2009a.

Gulley, J., Benn, D., Screaton, E., and Martin, J.: Mechanisms of englacial conduit formation and their implications for subglacial recharge, Quaternary Science Reviews, 28, 1984–1999, https://doi.org/10.1016/j.quascirev.2009.04.002, 2009b.

Hansen, L. U., Piotrowski, J. A., Benn, D. I., and Sevestre, H.: A cross-validated three-dimensional model of an englacial and subglacial
425   drainage system in a High-Arctic glacier, Journal of Glaciology, pp. 1–13, https://doi.org/10.1017/jog.2020.1, 2020.

Hart, J. K., Rose, K. C., Clayton, A., and Martinez, K.: Englacial and subglacial water flow at Skálafellsjökull, Iceland derived from ground penetrating radar, in situ Glacsweb probe and borehole water level measurements, Earth Surface Processes and Landforms, 40, 2071–2083, https://doi.org/10.1002/esp.3783, 2015.

Hock, R., Iken, L., and Wangler, A.: Tracer experiments and borehole observations in the over-deepening of Aletschgletscher, Switzerland,
430   Annals of Glaciology, 28, 253–260, https://doi.org/10.3189/172756499781821742, 1999.

Hooke, R. L. and Pohjola, V. A.: Hydrology of a segment of a glacier situated in an overdeepening, Storglaciaren, Sweden, Journal of Glaciology, 40, 140–148, 1994.

Huss, M. and Farinotti, D.: Distributed ice thickness and volume of all glaciers around the globe, Journal of Geophysical Research: Earth Surface, 117, 1–10, https://doi.org/10.1029/2012JF002523, 2012.

435   Iken, A. and Bindschadler, R. A.: Combined measurements of Subglacial Water Pressure and Surface Velocity of Findelengletscher, Switzerland: Conclusions about Drainage System and Sliding Mechanism, Journal of Glaciology, 32, 101–119, https://doi.org/10.3189/S0022143000006936, 1986.

Iken, A., Fabri, K., and Funk, M.: Water storage and subglacial drainage conditions inferred from borehole measurements on Gornergletscher, Valais, Switzerland, Journal of Glaciology, 42, 233–245, 1996.

440   Irvine-Fynn, T. D. L., Moorman, B. J., Williams, J. L. M., and Walter, F. S. A.: Seasonal changes in ground-penetrating radar signature observed at a polythermal glacier, Bylot Island, Canada, Earth Surface Processes and Landforms, 31, 892–909, https://doi.org/10.1002/esp.1299, http://doi.wiley.com/10.1002/esp.1299, 2006.

King, E. C., Woodward, J., and Smith, A. M.: Seismic evidence for a water-filled canal in deforming till beneath Rutford Ice Stream, West Antarctica, Geophysical Research Letters, 31, 4–7, https://doi.org/10.1029/2004GL020379, 2004.

445   Langhammer, L., Rabenstein, L., Bauder, A., and Maurer, H.: Ground-penetrating radar antenna orientation effects on temperate mountain glaciers, Geophysics, 82, H15–H24, https://doi.org/10.1190/geo2016-0341.1, 2017.

Lliboutry, L.: Permeability, Brine Content and Temperature of Temperate Ice, Journal of Glaciology, 10, 15–29, https://doi.org/10.1017/S002214300001296X, 1971.

Mercanton, P.: Vermessungen am Rhonegletscher/ Mensuration au glacier du Rhone: 1874-1915., vol. 52, Zürcher & Furrer, 1916.

450 Moorman, B. J. and Michel, F. a.: Glacial hydrological system characterization using ground-penetrating radar, Hydrological Processes, 14, 2645–2667, https://doi.org/10.1002/1099-1085(20001030)14:15<2645::AID-HYP84>3.0.CO;2-2, 2000.

Murray, T., Stuart, G. W., Gamble, N. H., and Crabtree, M. D.: Englacial water distribution in a temperature glacier from surface and borehole radar velocity analysis, Journal of Glaciology, 46, 389–398, https://doi.org/10.3189/172756500781833188, 2000.

Naegeli, K., Lovell, H., Zemp, M., and Benn, D. I.: Dendritic subglacial drainage systems in cold glaciers formed by cut-and-closure
455 processes, Geografiska Annaler, Series A: Physical Geography, 96, 591–608, https://doi.org/10.1111/geoa.12059, 2014.

Nienow, P., Sharp, M., and Willis, I.: Temporal Switching Between Englacial and Subglacial Drainage Pathways: Dye Tracer Evidence from the Haut Glacier D'arolla, Switzerland, Geografiska Annaler: Series A, Physical Geography, 78, 51–60, https://doi.org/10.1080/04353676.1996.11880451, 1996.

Nienow, P., Sharp, M., and Willis, I.: Seasonal changes in the morphology of the subglacial drainage system, Haut Glacier d'Arolla,
460 Switzerland, Earth Surface Processes and Landforms, 23, 825–843, https://doi.org/10.1002/(SICI)1096-9837(199809)23:9<825::AID-ESP893>3.0.CO;2-2, 1998.

Pettersson, R., Jansson, P., and Holmlund, P.: Cold surface layer thinning on Storglaciären, Sweden, observed by repeated ground penetrating radar surveys, Journal of Geophysical Research: Earth Surface, 108, n/a–n/a, https://doi.org/10.1029/2003JF000024, 2003.

Plewes, L. A. and Hubbard, B.: A review of the use of radio-echo sounding in glaciology, Progress in Physical Geography, 25, 203–236,
465 https://doi.org/10.1177/030913330102500203, 2001.

Reynolds, J. M.: An Introduction to Applied and Environmental Geophysics, John Wiley & Sons, 2011.

Roethlisberger, H.: Seismic Exploration in Cold Regions, 1972.

Röthlisberger, H.: Water Pressure in Intra- and Subglacial Channels, Journal of Glaciology, 11, 177–203, https://doi.org/10.1017/S0022143000022188, 1972.

470 Russell, B. H.: Introduction to Seismic Inversion Methods, Society of Exploration Geophysicists, https://doi.org/10.1190/1.9781560802303, 1988.

Rutishauser, A., Maurer, H., and Bauder, A.: Helicopter-borne ground-penetrating radar investigations on temperate alpine glaciers: A comparison of different systems and their abilities for bedrock mapping, GEOPHYSICS, 81, WA119–WA129, https://doi.org/10.1190/geo2015-0144.1, 2016.

475 Sacchi, M. D.: Reweighting strategies in seismic deconvolution, Geophysical Journal International, 129, 651–656, https://doi.org/10.1111/j.1365-246X.1997.tb04500.x, 1997.

Schaap, T., Roach, M. J., Peters, L. E., Cook, S., Kulessa, B., and Schoof, C.: Englacial drainage structures in an East Antarctic outlet glacier, Journal of Glaciology, https://doi.org/10.1017/jog.2019.92, 2019.

Schmelzbach, C. and Huber, E.: Efficient deconvolution of ground-penetrating radar data, IEEE Transactions on Geoscience and Remote
480 Sensing, 53, 5209–5217, https://doi.org/10.1109/TGRS.2015.2419235, 2015.

Schmelzbach, C., Tronicke, J., and Dietrich, P.: High-resolution water content estimation from surface-based ground-penetrating radar reflection data by impedance inversion, Water Resources Research, 48, 1–16, https://doi.org/10.1029/2012WR011955, 2012.

Seaberg, S. Z., Seaberg, J. Z., Hooke, R. L., and Wiberg, D. W.: Character of the Englacial and Subglacial Drainage System in the Lower Part of the Ablation Area of Storglaciären, Sweden, as Revealed by Dye-Trace Studies, Journal of Glaciology, 34, 217–227,
485 https://doi.org/10.3189/S0022143000032263, 1988.

Shreve, R. L.: Movement of Water in Glaciers, Journal of Glaciology, 11, 205–214, https://doi.org/10.3189/S002214300002219X, 1972.

Stuart, G.: Characterization of englacial channels by ground-penetrating radar: An example from austre Brøggerbreen, Svalbard, Journal of Geophysical Research, 108, 2525, https://doi.org/10.1029/2003JB002435, 2003.

Temminghoff, M., Benn, D. I., Gulley, J. D., and Sevestre, H.: Characterization of the englacial and subglacial drainage system in a high

490   Arctic cold glacier by speleological mapping and ground-penetrating radar, Geografiska Annaler, Series A: Physical Geography, 101, 98–117, https://doi.org/10.1080/04353676.2018.1545120, 2019.

Tsutaki, S., Sugiyama, S., Nishimura, D., and Funk, M.: Acceleration and flotation of a glacier terminus during formation of a proglacial lake in Rhonegletscher, Switzerland, Journal of Glaciology, 59, 559–570, https://doi.org/10.3189/2013JoG12J107, 2013.

van der Veen, C. J.: Fracture propagation as means of rapidly transferring surface meltwater to the base of glaciers, Geophysical Research

495   Letters, 34, 1–5, https://doi.org/10.1029/2006GL028385, 2007.

Velis, D. R.: Stochastic sparse-spike deconvolution, Geophysics, 73, R1–R9, https://doi.org/10.1190/1.2790584, 2008.

Warren, C., Giannopoulos, A., and Giannakis, I.: gprMax: Open source software to simulate electromagnetic wave propagation for Ground Penetrating Radar, Computer Physics Communications, 209, 163–170, https://doi.org/10.1016/j.cpc.2016.08.020, http://dx.doi.org/10.1016/j.cpc.2016.08.020, 2016.

500 Widess, M. B.: How thin is a bed?, Geophysics, 38, 1176–1180, https://doi.org/10.1190/1.1440403, 1973.

Zwally, H. J., Abdalati, W., Herring, T., Larson, K., Saba, J., and Steffen, K.: Surface melt-induced acceleration of Greenland ice-sheet flow, Science, 297, 218–222, https://doi.org/10.1126/science.1072708, 2002.